Annealing process in quenched Al-Sn alloys: A positron annihilation study

Jakub Čížek,* Oksana Melikhova, Ivan Procházka, Jan Kuriplach, Ivana Stulíková, and Petr Vostrý[†]

Faculty of Mathematics and Physics, Charles University, V Holešovičkách 2, CZ-18000 Prague 8, Czech Republic

Jiří Faltus

Research Institute of Metals, Panenské Břežany 50, CZ-25070 Odolena Voda, Czech Republic

The precipitation of tin atoms and vacancy-tin interaction in the diluted (800 at. ppm) Al-Sn alloy were studied by means of positron-lifetime and coincidence Doppler broadening techniques. In particular, the specimen subjected to the solution treatment at 525 °C/2 h finished by the rapid quenching down to room temperature was examined and, furthermore, the stability of the as-quenched microstructure at room temperature was tested. At room temperature we observed Sn atoms bound to quenched-in excess vacancies. Subsequently, the specimen was isochronally annealed up to the temperature of the solution treatment and the processes, which take place when increasing the temperature, were investigated. Among others, we could monitor the Sn nanoclusters' formation that starts at about 130 °C. Positron measurements were complemented by calculations of several positron characteristics of Al, Sn, and related defects in order to ensure the consistent interpretation of experimental data.

I. INTRODUCTION

Investigations of the decomposition of supersaturated solid solutions represent an important task both from physical and practical points of view.[1] In particular, it is highly desirable to understand the formation of solute atom aggregates/precipitates, their structure, and their interaction with the host in dependence on quenching and aging conditions. Such investigations are, in principle, difficult to perform because of a very small spatial scale (nanoscale) involved which may comprise individual atoms and/or vacancies. Positron annihilation (PA) spectroscopy[2,3] (PAS) may substantially help in such studies due to its high sensitivity to open volume defects as well as to embedded nanoparticles. The sensitivity to nanoparticles has been illustrated, for example, in the Fe-Cu (Ref. 4) and MgO-Li (Ref. 5) systems. Vacancy-solute complexes have been also examined by PAS. As an example, we mention that several Fe-based alloys have been investigated by Nagai *et al.*[6] and Al-Cu-Mg alloys have been studied by Biasini *et al.*[7] and by Nagai *et al.*[8]

Al-based alloys attract wide attention because of their frequent industrial applications that stem from a low specific density of aluminum whose mechanical properties are enhanced by fine dispersed particles due to alloying elements. Such alloys are referred to as age-hardenable alloys.[9] The mechanism of aggregation/precipitation of alloying elements is still a physically fundamental issue with many unsolved questions. One of the most frequently studied age-hardening systems is the Al-Cu one. It is because Al-Cu represents a typical system where precipitation starts from the formation of Guinier-Preston (GP) zones.[1,10]

The purpose of the present work is to study the Al-Sn system as a basis for understanding the role of Sn in more complex systems that can be employed in industrial applications. In particular, it was shown[11] that it is possible to replace toxic lead by nontoxic tin in Al-Cu-Bi-Pd alloy, which

is one of the most common machinable wrought Al-based alloys. Nevertheless, contrary to Pb the decomposition sequence of Al-Cu is substantially influenced by the presence of even a small amount of Sn.[12] Thus, the information obtained in the present work on the binary Al-Sn system should help in getting insight into the processes which take place during annealing of more complex Al-Cu-Sn–based alloys.

The atomic volume of Sn is almost twice that of Al. Thus, it is hard to accommodate a tin atom in the aluminum matrix, which is manifested by a very low solubility of Sn in Al.[13] Tin atoms can be coupled to vacancies and other open volume defects with a relatively high binding energy. For example, a binding energy of 0.4 eV of Sn to a monovacancy was reported.[14,15] The strong interaction between Sn atoms and vacancies results in a shift of the post-quenched recovery of vacancies in diluted Al-Sn alloys towards remarkably higher temperatures than in pure Al as shown by electrical resistometry.[14,15]

The vacancy-tin interaction was also studied by several authors[16–20] using Mössbauer spectroscopy. This technique brings an interesting information about the state and surrounding of tin atoms. However, there are significant differences among both the results and interpretations given in these works. We note that the Sn content and quenching rate differ from work to work. It is a common result of all the works[16–20] that the line with the isomer shift $I_s=2.0 -2.2$ mm/s was found in the quenched specimens. There also seems to be an agreement among the authors[16–20] that this line represents a contribution of Sn-vacancy pairs. In addition, another line with $I_s=2.8-2.9$ mm/s was resolved in all the studies. This component was attributed to Sn atoms coupled to vacancy aggregates.[17,20] On the other hand, it was suggested by others that this line comes from clusters of Sn atoms.[16,19] In addition, a line with $I_s=2.3$ mm/s attributed to dissolved tin atoms was found by several authors[16,18] in quenched specimens.

PAS was successfully used many times in studies of the defect structure in Al-based age-hardenable alloys (see Ref. 21 for a review). To our knowledge, two positron lifetime (PL) studies of the Al-Sn system have been performed so far.[19,20] However, the annealing behavior of Al-Sn was investigated at relatively low temperatures only. Moreover, PL spectrometers with a relatively poor timing resolution (more than 300 ps) were employed. This makes it difficult to resolve short and/or weak components in measured PL spectra. A lifetime of ~246 ps was found in the quenched specimen.[19] This lifetime corresponds to positrons trapped in Al monovacancies.[22,23] On the other hand, only a single component with a lifetime of ~265 ps was resolved in the PL spectrum of the quenched Al-Sn alloy in Ref. 20. Hence, the abovementioned studies do not allow one to draw unambiguous conclusions about defects in the Al-Sn system and it is therefore desirable to continue with PA studies of this system and find out other details about its defect structure using advanced experimental PA techniques such as high-resolution PL spectroscopy and coincidence Doppler broadening (CDB) spectroscopy. We prefer these methods over conventional techniques—such as transmission electron microscopy (TEM)—due to a very small size of nanoparticles involved and an important role played by vacancies which are hardly detectable using conventional techniques. Moreover, when compared to Mössbauer spectroscopy PL spectroscopy directly monitors the vacancies and their clusters. In addition, the CDB technique can provide the direct information on the atomic (chemical) environment of studied open volume defects.[7,24,25]

The main aim of the present work is to study carefully the microstructure of a diluted Al-Sn alloy quenched rapidly from the solution treatment temperature and the vacancy assisted clustering of Sn atoms in a broad range of temperatures. More specifically, for the quenched system we intended to clarify several open questions which seem not to be resolved by Mössbauer spectroscopy. (i) Is dissolved tin distributed homogeneously or does it form some clusters? (ii) Are Sn atoms coupled with monovacancies or vacancy clusters? (iii) What is the stability of the quenched microstructure at room temperature? Furthermore, we study the development of the quenched microstructure with increasing temperature during isochronal annealing from the room up to the solution treatment temperature. Finally, we also examine a slowly cooled specimen. Measurements are accompanied by calculations of positron quantities of interest for Al, Sn, and related defects, which helps us to interpret the experimental data properly.

The paper is organized as follows. We first give a description of the examined Al-Sn samples and PL and CDB experimental techniques (Sec. II). Positron calculations and their results are described in Sec. III. Then, we continue with the obtained experimental results and discussions of various microstructural aspects of the studied Al-Sn system (Sec. IV). The paper is concluded in Sec. V.

II. EXPERIMENTAL DETAILS

A. Specimens

The studied Al-Sn (800 at. ppm) alloy was prepared in The Research Institute of Metals, Panenské Břežany, Czech

TABLE I. The chemical composition of the studied Al-Sn alloy (at. %).

Al	Sn	Fe	Si	Pb	Bi
balance	0.080	0.063	0.060	<0.001	0.013

Republic. Extruded specimens were subjected to the solution treatment at 525 °C for 2 h at a vertical furnace with the argon protective atmosphere and then rapidly quenched into water of room temperature. After quenching the specimens were quickly transferred into a bath of liquid nitrogen where they were stored until measurement. Subsequent isochronal annealing was performed by heating samples in steps of 20 °C/20 min. The annealing was carried out in a silicon oil bath (below 250 °C) and in the vertical furnace with the argon protecting atmosphere (above 250 °C). Each annealing step was finished by rapid quenching into water of room temperature.

The chemical composition of samples is given in Table I. There is a significant concentration of Fe and Si which represent most common impurities in commercial Al-based alloys. A possible influence of these impurities on the studied processes as well as on the measured positron characteristics will be discussed in detail below. We state beforehand that their influence appears to be negligible.

B. Positron-lifetime spectroscopy

A PL spectrometer based on the fast-slow one described in Ref. 26 was employed in the present work. The spectrometer[26] was recently modified[27,28] with the purpose to enhance the coincidence count rate keeping simultaneously excellent timing resolution of the device. The timing resolution of the spectrometer was 150 ps [full width at half maximum (FWHM)] for a ^{22}Na source of an activity of ~1.3 MBq at a typical coincidence counting rate of 75 s^{-1}. The ^{22}Na positron source was sealed between two mylar foils of 2 μm thickness. The source contribution, which arises from positron annihilations in the positron source and the mylar foils, consisted of two components with lifetimes 368 ps and 1.5 ns and relative intensities 9 and 1 %, respectively. The parameters of the source components were obtained using a reference sample of high purity well annealed (defect free) Al (99.9999%). The shorter source component was fixed in the analysis of PL spectra of Al-Sn samples. It was not necessary to fix the long-lived source component because it is well separated from the other components. PL measurements were performed at room temperature and at least 10^7 counts were collected in the spectrum for each annealing temperature. In the case of the slowly cooled sample (Sec. IV G) PL spectrum with lower statistics (4×10^6 counts) was collected. Measured spectra were decomposed by means of a maximum-likelihood procedure[29] into up to four exponential components. The time-resolution function of the spectrometer was considered as a sum of three Gaussians and was fitted simultaneously with other parameters (for details see Refs. 27 and 29).

TABLE II. The results of calculations of positron affinity (A_+) and bulk lifetime (τ_B) for Al and β-Sn. Experimental bulk lifetimes are collected in the seventh column. Lifetimes (τ_V) of positrons trapped at vacancies are also specified (ATSUP technique) together with their experimental counterparts (if available). Columns with computed quantities are labelled with the abbreviations of the computational method and the form of the positron correlation/enhancement used.

Element	LMTO-BN A_+ (eV)	LMTO-BN τ_B (ps)	LMTO-GGA A_+ (eV)	LMTO-GGA τ_B (ps)	ATSUP-BN τ_B (ps)	experimental τ_B (ps)	ATSUP-BN τ_V (ps)	experimental τ_V (ps)
Al	−4.8	163	−4.6	153	167	163±5 (Ref. 39)	240	239 (Ref. 23)
β-Sn	−6.8	185	−6.4	188	187	202±5 (Ref. 39)	274	

C. Coincidence Doppler broadening spectroscopy

The coincidence Doppler broadening (CDB) spectrometer employed in the present work consisted of two HPGe detectors and commercial NIM modules operated by a PC. The energy resolution of the spectrometer was 1.2 keV (FWHM) at 511 keV energy and the coincidence count rate amounted to ~650 s^{-1} for a 1 MBq ^{22}NaCl positron source (sealed between 2-μm-thick mylar foils). At least 10^8 events were collected in each two-dimensional spectrum, which was subsequently reduced into the one-dimensional Doppler profile and instrumental resolution cuts. In order to inspect the nature of positron annihilation sites, relative changes of Doppler profiles were followed as ratios of the profiles normalized to the same area to a proper reference profile normalized to the same area as well. The reference profile was taken to be well annealed. (defect free) high purity aluminum (99.9999%).

III. POSITRON CALCULATIONS

Calculations of positron quantities of interest may substantially help when interpreting positron measurements. Such calculations bring not only the quantitative characterization of the positron response from a studied system and its defects, but the microscopic origin of this response is also accessible. In defect studies it is not often obvious whether a given defect represents a positron trap and/or what are its positron characteristics. Thus, in order to test whether the Sn precipitates in Al represent attractive sites for positrons, calculations of the positron affinity for Sn and Al were performed. In addition, we calculated positron lifetimes for bulk Al and Sn and single vacancies in these materials to be able to distinguish between vacancies in Al and Sn. We also examined the high momentum parts (HMPs) of the momentum distribution of annihilation γ-quanta for several vacancy-tin complexes in Al. In general, HMPs provide the information about the annihilation of positrons with core electrons. This will be helpful in the next section when identifying the atomic environment of annihilation sites.

The so-called vanishing positron density limit[30,31] was adopted in the calculations of positron properties. We employed two computational techniques. First, it is the linear muffin-tin orbital (LMTO) method[32] within the atomic-sphere approximation[32] (ASA). Calculations of selected quantities were also carried out using the so-called atomic

superposition (ATSUP) method.[33,34] To compare the two used techniques, the ATSUP method is not self-consistent and neglects charge transfer effects in contrast to the LMTO technique. On the other hand, the ATSUP method retains fully the three-dimensional geometry of the studied system whereas the electron density and potential are spheridized in the vicinity of atomic sites within the LMTO framework. In some respect these two techniques are complementary and we use them both in order to check the adequacy of approximations employed in them by comparing their results.

In our calculations the correlation part of the positron potential[30,31] was determined using the parametrization obtained by Boroński and Nieminen[35] (BN) within the framework of the local-density approximation for positrons.[35] For the sake of comparison, we also applied the formula introduced recently by Barbiellini et al.[36] based on the generalized gradient approximation (GGA) for electron-positron correlations. Once the positron potential is known, a Schrödinger-like equation[30,31] is solved to find the positron ground state and energy.

The LMTO method was used to calculate positron affinities and bulk positron lifetimes. The ATSUP method was also used for the latter as well as for vacancy lifetimes. The calculation of HMPs was carried out using this method, too. The details of the positron affinity and positron lifetime calculations can be found in Ref. 37. The HMPs were computed according to the scheme described in Ref. 38 using the GGA.[36] In these calculations the following core electron configurations were considered: for Al the Ne core was taken and for Sn the Kr core$+4d^{10}$ configuration was adopted. We further note that calculated HMP profiles were normalized[38] in the way that their total areas were set to be $\lambda_{core}/\lambda_{total}$ times the area used to normalize experimental CDB spectra (see Sec. II C). Here, λ_{core} and λ_{total} are, respectively, calculated core and total annihilation rates for a given case.

The crystal structures taken into account in calculations are face centered cubic and tetragonal for Al and β-Sn, respectively. A vacancy is simply created by removing one atom from 256 atom supercells used both for Al and Sn (of course, atomic positions in Al differ from those in Sn). No lattice relaxations around vacancies were considered at this stage.

The results of calculations are collected in Table II. The obtained results for Al agree well with those presented in the literature.[31,33,36] In the case of tin, only preliminary results for the bulk lifetime were presented in Ref. 40. To our

knowledge, the positron affinity and vacancy lifetime for β-tin were not calculated before. Clearly, the positron affinity of Sn is positioned substantially lower than that for Al. This means that Sn precipitates are attractive for positrons.[31] In principle, this approach should be used for large Sn particles only as they can be considered as a separate phase and the positron affinity is a well-defined quantity for them. On the other hand, our recent study[41] indicates that even for very small particles the affinity approach can reasonably be used. Thus, the minimum precipitate radius r_c to have a bound positron state can be roughly estimated from the equation[42]

$$r_c[\text{Å}] = 3.1/\sqrt{\Delta A_+[\text{eV}]}, \qquad (1)$$

where $\Delta A_+ > 0$ represents the positron affinity difference between the matrix and the precipitate. Using the calculated affinities (Table II) we obtain the minimum radius of Sn precipitates $r_c \approx 2$ Å. This is a very small radius which results in a volume smaller than the Sn atomic volume. Hence we conclude that even very small clusters of Sn atoms may probably act as a trapping site for positrons. Lifetime results will be discussed below, in the context of experimental results.

In order to examine the nature of vacancylike defects in the Al-Sn system, we also calculated positron characteristics of atomic configurations of several such defects. Namely, these are vacancy-Sn (V-Sn), divacancy-Sn (V_2-Sn), and vacancy-Sn_2 (V-Sn_2) complexes and nondecorated vacancy. Their atomic configurations were obtained using the Vienna *ab initio* program[43–45] (VASP) developed at the Institut für Materialphysik of the Universität Wien. In all calculations 108 atom based cells ($3 \times 3 \times 3$ fcc units of Al) were employed. The starting configurations were created so that a vacancy corresponds to a missing Al atom; Sn atoms were put into Al lattice sites. For all defects nearest-neighbor configurations of vacancies and Sn atoms were considered. The relaxed defect configurations were obtained by minimizing the total energy of the supercell with respect to atomic positions. The calculated binding energy of the V-Sn complex is 0.2 eV, which is somewhat smaller value than that found experimentally. The reason for this discrepancy could be yet insufficient size of supercells used in calculations. In the following we shall use the experimental value 0.4 eV.[14,15] For ATSUP positron calculations we used 500 atom based supercells created from the original (VASP) ones by adding atoms at the sides to minimize an influence of boundary conditions.[46] These added atoms were arranged in the form of the regular Al fcc lattice.

As expected, relaxations around defects—except for the single vacancy—are quite large, which is documented in Table III. For example, in the case of the V-Sn complex the Sn atom is moved towards the vacancy after the relaxation process whereas surrounding Al atoms are pushed away from the Sn atom. A similar situation occurs for the V_2-Sn complex. Calculated positron lifetimes and W parameters are also specified in Table III. One can see that the positron lifetimes for all studied defects are nearly the same and around 240 ps (see Table II). This can be somewhat surprising for the V_2-Sn defects as the divacancy in Al gives a lifetime of about 270 ps (Ref. 33), but the large atomic relaxations around V_2-Sn

TABLE III. Properties of relaxed vacancylike defects in the Al-Sn system. Relaxations are given in percents of the Al lattice constant; the first (second) number is the largest deviation of Al (Sn) atoms with respect to their original positions (given by the ideal Al lattice).

	V	V-Sn	V_2-Sn	V-Sn_2
relaxation (%)	0.6	2.8; 5.0	3.7; 9.1	3.1; 3.8
lifetime (ps)	240	236	248	236
W parameter	0.00212	0.00263	0.00257	0.00291

reduce the free volume and consequently the positron lifetime. Thus, the positron lifetime can hardly be used to differentiate among studied defects. A measurement of the CDB/HMP profiles should be more sensitive to the vacancy environment. This can be clearly seen from the calculated values of the W parameter (Table III). Namely, the presence of Sn apparently results in an increase of W. The W parameter was determined by integrating the calculated HMP profiles in the ranges of Doppler profiles where 4 KeV $< |\Delta E| > 6$ KeV (see Fig. 1). This parameter characterizes predominantly PA with core electrons.

The calculated HMP profiles for pure Sn and examined vacancylike defects with respect to Al are shown in Fig. 1. The ratio profile of Sn deviates significantly from the straight line at the level 1 (that represents Al). This again gives an indication that a vacancy decorated by a Sn atom could be distinguished from a nondecorated vacancy. Indeed, the ratio curves for decorated vacancies (or a divacancy) exhibit a signature of Sn that is a minimum of the ratio curve at about 7 KeV. The increase of the W-parameter for decorated vacancies compared to the nondecorated one, as mentioned above, can also be understood from Fig. 1. On the other hand, the mutual differences among ratio curves corresponding to decorated (di)vacancies are rather small and for the purpose
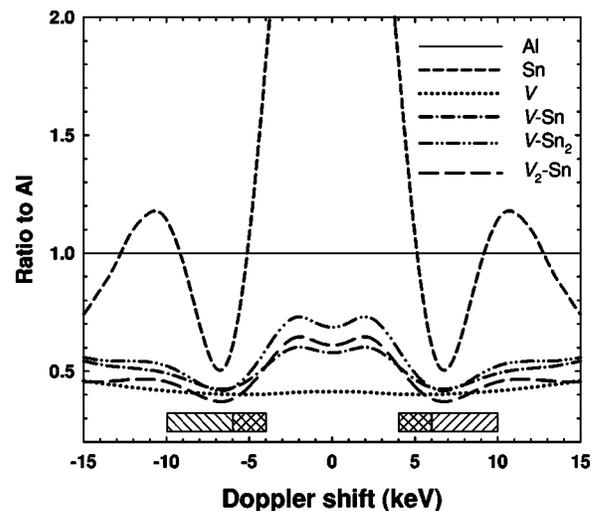
FIG. 1. Ratio HMP profiles of Sn and vacancylike defects with respect to Al. The crosshatched areas mark energy regions used for W-parameter calculation; the whole filled areas (hatched +crosshatched) mark regions used for comparison with experiment.
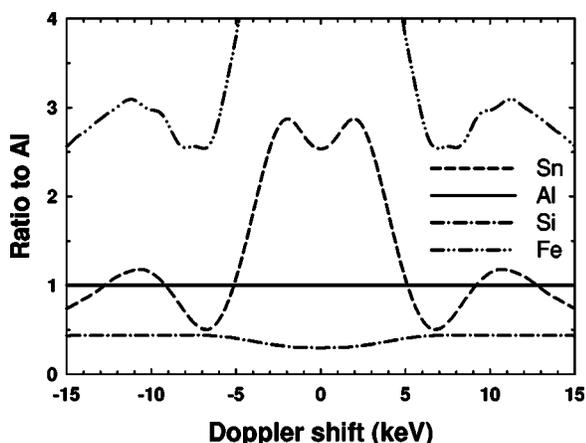
FIG. 2. Ratio HMP profiles of Sn, Si, and Fe with respect to Al.

FIG. 3. The positron mean lifetime as a function of the annealing temperature.

of comparison of experiment and calculations we consider only the V-Sn complex in the following. We note that for a comparison with experiment Doppler shift regions $|\Delta E| \gtrsim 4$ keV should be considered only (see Fig. 1) and such a comparison for Doppler shifts $|\Delta E| \lesssim 3$ keV is definitely meaningless, especially for ratio profiles, because of the missing valence electron contribution in HMP profiles.

Finally, we discuss a possible effect of other impurity atoms (Si, Fe) in the studied alloy on CDB/HMP spectra. The spectra were calculated using the ATSUP method as explained above. In calculations the bcc and diamond structures of Fe and Si were considered, respectively. The core electron configurations were as follows: for Fe the Ar core $+3d^6$ was taken and for Si (as for Al) the Ne core configuration was adopted. The ratio curves for Sn, Si, and Fe with respect to Al are plotted in Fig. 2. The curves for Si and Fe apparently differ from that for Sn. In particular, the electron configuration of Sn is similar to that of Si, but Sn has $4d$ electrons that result in a maximum at about 11 keV (not present in the Si curve). A similar maximum is also present in the Fe profile, which is due to $3d$ electrons of Fe, but the corresponding curve is positioned much higher than that for Sn (and Si). Hence, if Si and Fe would precipitate and/or interact with vacancies, their effect should be visible in measured CDB profiles, which will be further discussed in the context of experimental results presented below.

IV. RESULTS AND DISCUSSION

A. Positron lifetime measurements

The positron mean lifetime represents the center of mass of a PL spectrum and it is therefore a robust parameter independent of the number of components, constraints involved in the fitted model as well as correlations among parameters. The mean positron lifetime for the quenched specimen is 206 ps. The dependence of the mean lifetime on the annealing temperature is shown in Fig. 3. As one can see, the mean lifetime increases starting from a temperature of 130 °C and reaches its maximum at 200 °C. Above 200 °C, the mean lifetime exhibits a pronounced decrease up to its minimum at
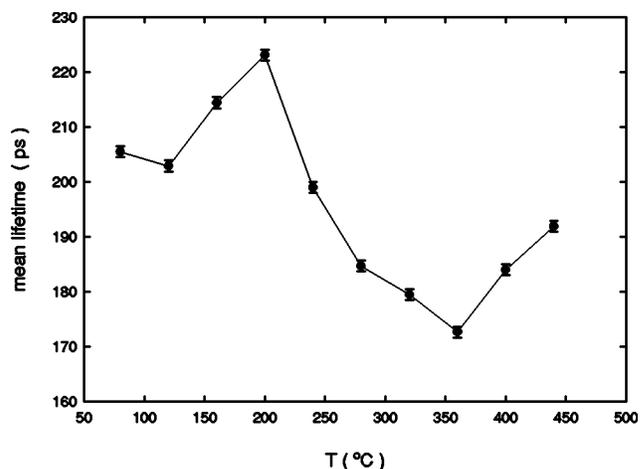
360 °C. Subsequently, it increases again for annealing temperatures higher than 360 °C. The mean lifetime is higher than the aluminum bulk lifetime $\tau_B = 163$ ps (Ref. 39, Table II). This clearly shows the presence of trapping sites in the studied alloy.

The measured lifetime spectrum of the quenched specimen can be well decomposed into two lifetime components that are as follows: $\tau_1 = 88 \pm 4$ ps and $\tau_2 = 235 \pm 5$ ps with the corresponding intensities $I_1 = 20 \pm 2\%$ and $I_2 = 80 \pm 2\%$ (note that relative intensities are normalized so that $I_1 + I_2 = 100\%$). The lifetime τ_1 of the first component is remarkably lower than $\tau_B = 163$ ps mentioned above. Therefore, we attributed this component to free positrons. The second component comes from positrons trapped at defects. A comparison with above presented results of positron calculations gives an indication that positrons—apart from the delocalized state—annihilate in vacancylike defects having a size of about one vacancy.

All measured PL spectra of the annealed sample can be again well fitted by two exponential components (except for the source contribution). Lifetimes τ_1 and τ_2 of the spectral components are plotted as functions of the annealing temperature in Fig. 4. The dependence of the relative intensity I_2 of the second component on the temperature is shown in Fig. 5.

As in the quenched specimen, we attributed the first component to free positrons. The second component originates from positrons annihilating at defects. The τ_2 lifetime of the latter component increases from ~240 to ~270 ps in the temperature interval 130–200 °C. We note that χ^2 reduced to the number of degrees of freedom ν amounts to 1.05 and 1.22 for a fit of the PL spectrum corresponding to 200 °C with τ_2 as a free parameter and τ_2 fixed to 240 ps, respectively. The former fit resulted in $\tau_2 = (275 \pm 4)$ ps. The expected standard deviation $\sigma = \sqrt{2/\nu}$ of the χ^2 distribution reduced to the number of degrees of freedom is 0.03. The substantial increase of χ^2 for the fit with τ_2 fixed at 240 ps clearly indicates that the increase of τ_2 in this temperature range is indeed statistically significant.
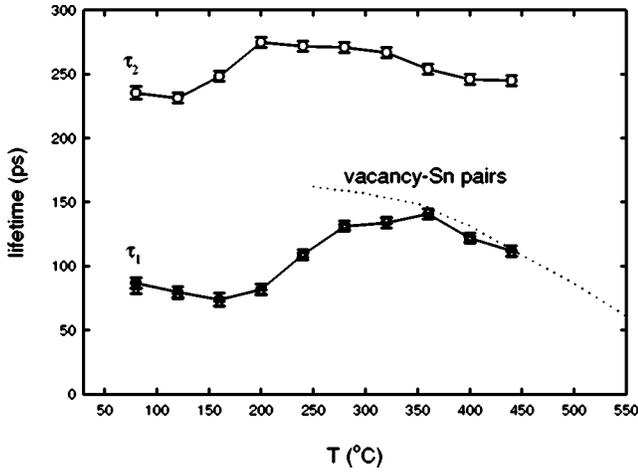
FIG. 4. The dependence of positron lifetimes on the annealing temperature: -•- the lifetime τ_1 of free positrons, -○- the lifetime τ_2 of trapped positrons, Δ - the lifetime τ_1^{STM} calculated using the STM (see the text for details). The lifetime τ_1 calculated using the assumption that positrons are trapped at vacancy-Sn pairs formed during annealing is plotted by the dotted line (see Sec. IV F).

Subsequently, τ_2 remains roughly constant and above 350 °C it eventually decreases back to ~240 ps. The relative intensity I_2 is approximately constant up to 160 °C, then it decreases drastically in the temperature interval 160–360 °C (see Fig. 5). Finally, above 360 °C it remarkably increases again. In the following sections we will examine various possibilities for positron trapping sites in the Al-Sn alloy.

We now check the above assumption that measured lifetime spectra can be decomposed into two components (apart from the source contribution). For this purpose we use the two-state simple trapping model[42,47] (STM). The lifetime

$$\tau_1^{STM} = \frac{I_1 \tau_B \tau_2}{\tau_2 - I_2 \tau_B} \quad (2)$$

calculated from I_1, I_2, and τ_2, and $\tau_B = 163$ ps using the STM is labeled with open triangles in Fig. 4. In this figure the τ_1^{STM}
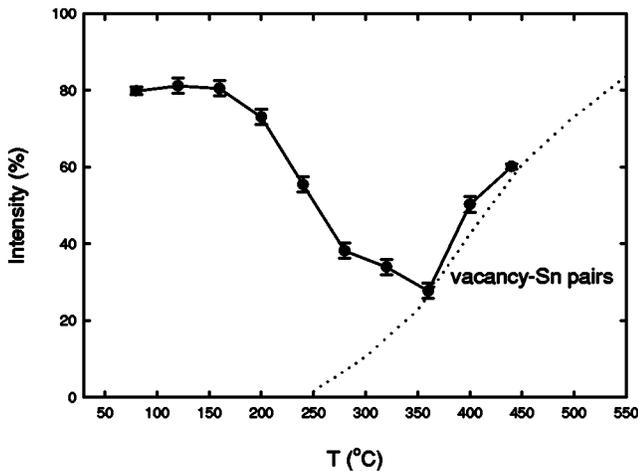
FIG. 5. The relative intensity I_2 of the component which belongs to trapped positrons. The calculated relative intensity of the component coming from positrons trapped at vacancy-Sn pairs formed during annealing is plotted by the dotted line (see Sec. IV F).

lifetimes agree well with the measured ones in the whole temperature range. Hence, the application of the two-state STM is justified in the present case and the decomposition of spectra to two components is physically plausible. The same holds for the quenched specimen.

B. Large Sn-rich particles

The solubility of Sn in Al is 200 at. ppm at a solution treatment temperature of 525 °C (see Ref. 13). As the studied specimens contain 800 at. ppm of Sn, particles of Sn-rich (64 at. % of Sn) phase[13] are formed in addition to the solid solution of Sn in Al during the solution treatment. After the annealing time $t=2$ h the mean diffusion length of Sn atoms

$$L_{Sn} = \sqrt{Dt} \quad (3)$$

appears to be ≈0.1 mm, which is clearly sufficient for the abovementioned redistribution of Sn atoms. The diffusion coefficient D of Sn in aluminum was taken from the recent work.[48] On the basis of the TEM study of an Al-Cu-Sn-Bi alloy, which contained the same amount of tin and was subjected to the identical solution treatment,[12] we conclude that the Sn-rich incoherent particles are large and their linear size is certainly significantly greater than 100 nm. Hence, it is possible to estimate the positron trapping rate to these Sn-rich particles. Clearly, positron trapping at these particles will be limited by the diffusion of positrons to the vicinity of their surface. Under the assumption of trapping at the surface of spherically shaped Sn-rich particles with the radius r, the positron trapping rate may be expressed as[49]

$$K_D = 4\pi r N D_+. \quad (4)$$

The volume concentration of particles is denoted by N. The symbol D_+ stands for the positron diffusion coefficient. For Al, $D_+ = 1.7$ cm^2 s^{-1} was reported.[42] According to the equilibrium Al-Sn phase diagram,[13] the number of Sn atoms forming Sn-rich particles at the solution treatment temperature is ≈600 at. ppm. The volume fraction N of particles is proportional to $1/r^3$. Thus, considering $2r=100$ nm as a lower limit of the Sn-rich particle diameter, from Eq. (4) we obtain an upper estimate of the positron trapping rate $K_D = 3.4 \times 10^8$ s^{-1}, which is more than one order of magnitude smaller than the bulk annihilation rate for aluminum $\lambda_B = 1/\tau_B \approx 6 \times 10^9$ s^{-1} (Refs. 22, 30, and 39). If we assume $\tau_2 \sim 240$ ps, the contribution of positron trapping at the Sn-rich particles will be smaller than 10% (when K_D is compared with the total trapping rate derived from the STM). Hence, the large Sn-rich particles do not represent significant positron traps that could explain the observed intensity I_2 and will be neglected in the following discussions.

C. Sn-vacancy pairs and Sn nanoparticles

A relatively high binding energy of 0.4 eV between vacancies and Sn atoms was determined experimentally.[14,15] Thermal vacancies can be, therefore, bound to dissolved Sn atoms during the solution treatment. As a consequence a significant amount of tin atoms can be coupled to vacancies after quenching (to room temperature) as also turned out

from the Mössbauer study[20] of the Al-Sn alloy. The migration of vacancies in pure Al takes place already below room temperature.[50,51] The "free" vacancies (not associated with Sn) are highly mobile and quickly disappear after and/or during quenching. Only vacancies bound to Sn atoms may "survive" quenching. As PAS measurements are performed at room temperature and positrons are obviously trapped at open volume defects, it is natural to expect that they are trapped at the vacancies bound to Sn atoms. The lifetime $\tau_2 \approx 240$ ps coincides with the lifetime of positrons trapped in the monovacancies in Al reported in the literature[22,23] (see Table II). One could thus argue that the second lifetime component comes from positrons trapped in monovacancies bound to Sn atoms. However, as discussed in Sec. III (Table III), the V_2-Sn and V-Sn$_2$ complexes exhibit lifetimes that are very close to that for the V-Sn complex. This means that on the basis of lifetime measurements one cannot unambiguously determine the defect responsible for a lifetime component of ~240 ps. Nevertheless, the size of the free volume associated with such defects is about the same as that of the monovacancy.

Let us now continue with thermodynamic considerations. The concentration of thermal-equilibrium vacancies is

$$c_V^* = \exp(S_V^f/k)\exp(-E_V^f/kT), \qquad (5)$$

where S_V^f and E_V^f denote the monovacancy formation entropy and enthalpy, respectively, and k stands for the Boltzman constant. For aluminum $S_V^f=1\,k$ (Refs. 52 and 53) and $E_V^f=0.6$ eV (Ref. 30) may be found in the literature. At $T=525$ °C, i.e., at the solution treatment temperature, the equilibrium concentration of vacancies $c_V^*=430$ at. ppm, is about two times higher than the concentration of dissolved tin atoms (200 at. ppm). The equilibrium concentration of vacancy-Sn pairs is then given by the expression

$$c_{V\text{-Sn}}^* = c_V^* \exp(E_b^{V\text{-Sn}}/kT)c_{\text{Sn}}^{\text{dissolved}}, \qquad (6)$$

where $E_b^{V\text{-Sn}}=0.4$ eV (Refs. 14 and 15) denotes the binding energy of a Sn atom to a vacancy and $c_{\text{Sn}}^{\text{dissolved}}=200$ at. ppm is the concentration of dissolved tin atoms at the temperature of the solution treatment. Equation (6) yields $c_{V\text{-Sn}}^*=30$ at. ppm. It means that about 15% of Sn atoms dissolved in the solid solution during the solution treatment are bound to vacancies. The equilibrium concentration of V-Sn$_2$ can be estimated from the expression

$$c_{V\text{-Sn}_2}^* \approx c_V^* \exp(2E_b^{V\text{-Sn}}/kT)(c_{\text{Sn}}^{\text{dissolved}})^2, \qquad (7)$$

which results in $c_{V\text{-Sn}_2}^* \approx 2$ at. ppm. The equilibrium concentration of V_2-Sn defects can be estimated in a similar way

$$c_{V_2\text{-Sn}}^* \approx (c_V^*)^2 \exp((E_b^{V\text{-Sn}}+E_b^{V\text{-}V})/kT)c_{\text{Sn}}^{\text{dissolved}}, \qquad (8)$$

where $E_b^{V\text{-}V}$ represents the binding energy of a divacancy in Al. The binding energy $E_b^{V\text{-}V}$ is not known, but we suppose that it should not be higher than $E_b^{V\text{-Sn}}$, i.e., 0.4 eV. Thus, we obtain an estimate that $c_{V_2\text{-Sn}}^* < 4$ at. ppm. Hence, it is clear that concentrations of the three-site defects V_2-Sn and

V-Sn$_2$ are significantly smaller than that of V-Sn pairs and they do not contribute significantly to the positron signal.

The concentration of vacancies in the quenched sample can be calculated from lifetimes and relative intensities obtained from the decomposition of the PL spectrum using the STM

$$c_{V\text{-Sn}}^{\text{quench}} = \frac{1}{\nu_V}\frac{I_2}{I_1}\left(\frac{1}{\tau_B}-\frac{1}{\tau_2}\right), \qquad (9)$$

where $\nu_V=2.5\times10^{14}$ at. s^{-1} is the specific positron trapping rate for monovacancies in Al.[42] Note that the specific trapping rate can be slightly changed for the vacancy-Sn pair due to the presence of the Sn atom. If we neglect this small difference in the present estimation, we obtain $c_{V\text{-Sn}}^{\text{quench}}=30\pm4$ at. ppm from Eq. (9). This number is in excellent agreement with the equilibrium concentration of vacancy-Sn pairs $c_{V\text{-Sn}}^*$ at the temperature of the solution treatment [see Eq. (6)]. Thus, we verified that the vacancy-Sn pairs formed during the solution treatment survived during quenching and are present in the quenched specimen, whereas vacancies not associated with Sn disappeared.

The Al-Sn equilibrium phase diagram[13] shows that the solubility limit of Sn in Al is negligible below the melting temperature of tin (230 °C). Notwithstanding the solubility can be extended by quenching, there are some indications coming from TEM,[12,18] Mössbauer spectroscopy,[19] and atom probe field ion microscopy[54,55] that very small Sn (nano)particles could be formed during quenching. The sizes of these particles of about 4 nm (Ref. 54) or smaller than 5 nm (Ref. 18) were reported. As shown in Sec. III, positrons can be trapped at such nanocrystalline Sn precipitates. However, the calculated lifetime of positrons trapped at defect-free Sn precipitates (see Table II) is remarkably lower than τ_2. Thus, positrons are probably trapped at vacancies associated with Sn atoms instead of defect-free Sn precipitates. However, some clustering of Sn atoms during quenching cannot be excluded on the basis of current PL results. Nevertheless, if fine Sn clusters would be formed, they should be associated with vacancies because the mobility of Sn-vacancy pairs in Al is remarkably higher than that of Sn atoms themselves and because of a high binding energy of vacancies to Sn atoms. The above two estimates of the concentration of V-Sn pairs give a strong indication that PA at V-Sn pairs dominates over annihilation at vacancies connected with Sn precipitates.

We now discuss a possible influence of Si and Fe impurity atoms (see Table I). The maximum solubility of Si in Al is 1.5 at. % at an eutectic temperature of 577 °C. It decreases down to 0.05 at. % at 300 °C (Ref. 13). Although rapid quenching extends Si solubility in Al, a weak precipitation of Si atoms may occur in the studied samples. There is a large scatter in the binding energies $E_b^{V\text{-Si}}$ of a vacancy to a Si atom reported in literature. A very low binding energy of only 0.07 eV, i.e., 6 times smaller than that to Sn, was found in Ref. 56. On the other hand, $E_b^{V\text{-Si}} \approx 0.2$ eV was reported in Ref. 57. Using Eq. (6) for Si instead of Sn, one obtains that the equilibrium concentration of vacancies bound to Si atoms at the solution treatment temperature lies in a range from 1 to 5 at.

ppm depending on the binding energy value used. Even the highest possible estimation of the V-Si pair concentration is still 6 times smaller than the concentration of excess vacancies measured in the quenched sample. On the other hand, the positron affinity of Si is below that of Al (Ref. 31 and Table II) and positron trapping at Si precipitates cannot be excluded in principle. As PAS is sensitive mainly to open-volume defects, such as vacancies, and positron trapping at precipitates does not seem to play a dominant role in the present study (at least in the quenched specimen), one can assume that Si impurities do not affect PAS results.

Finally, the Fe solubility in Al is only 0.025 at. % at room temperature.[58] The binding energy of a vacancy to an Fe atom embedded in the Al matrix estimated in Ref. 57 is 0.18 eV. From Eq. (6) for Fe instead of Sn, we obtain the equilibrium concentration of vacancies bound to Fe atoms lower than 2 at. ppm at the solution treatment temperature. Thus, vacancies bound to Fe atoms cannot represent a significant contribution to PL spectrum. The positron trapping at Fe precipitates is not possible due to a higher positron affinity of Fe compared to Al (see Ref. 31). Thus, due to similar reasons as for Si, one does not probably need to consider Fe impurities in the interpretation of PAS results. A weak interaction of vacancies with Fe and Si atoms is also indicated by the fact that both Fe and Si atoms have no or little effect on the vacancy-assisted formation of GP zones in Al-Cu alloys.[57,59]

D. Stability of quenched microstructure

The mean diffusion length of Sn atoms in Al at room temperature calculated from Eq. (3) is very small. For a time period of 24 h, i.e., the time scale typical for PL measurements, it amounts to $\sim$2 Å. This clearly indicates that Sn nanoclusters are formed only during quenching, while no additional movement of Sn atoms occurs at room temperature in the time scale of at least a few days. In order to check experimentally the stability of the quenched microstructure at room temperature, we recorded the PL spectrum of the specimen quenched from the solution treatment temperature in a number of independent steps. Each step took 30 min. The PL spectra obtained in these steps were analyzed independently in terms of the mean lifetime. The dependence of the mean lifetime on the measuring time is shown in Fig. 6. Indeed, the mean lifetime remains constant during the whole time of the measurement, which manifests that no change of the quenched microstructure occurs in the time scale of several days and even more.

E. Sn-vacancy pairs probed using CDB spectroscopy

In order to further elucidate the nature of defects identified so far as Sn-vacancy pairs, we examined the quenched specimen using the CDB spectrometer. We first show results of CDB measurements for the pure Al (99.9999%) reference sample and pure Sn (99.999%) sample. Figure 7 presents measured CDB spectra for Al and Sn together with their theoretical (HMP) counterparts. It should be stressed that the calculated profiles should be compared to the experimental ones only for Doppler shifts larger than about 4 keV as the
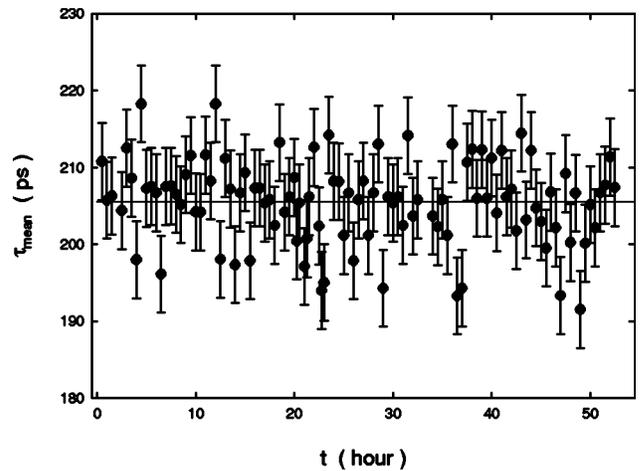
FIG. 6. The time dependence of the mean lifetime τ_{mean}. PL spectra were accumulated in a number of 30 min steps. The mean lifetime was calculated independently for the PL spectrum from each step.

valence electron contribution is neglected in calculated profiles (see also Fig. 1). Taking this into account one can realize that the calculated profiles match reasonably well the measured ones. In Fig. 8(a) we show the CDB ratio profile of Sn with respect to Al calculated using the data from Fig. 7. We note that in whole Fig. 8 we symmetrize the CDB data and plot only the part of CDB/HMP profiles corresponding to positive Doppler shifts. Clearly, the calculations reproduce well the minimum at about 7 keV Doppler shift in pure Sn though the calculated minimum is somewhat deeper (by about 0.2) than in the experimental profile.

The measured CDB ratio profile for the quenched specimen is presented in Fig. 8(b). On the basis of the simple trapping model[42] and using the lifetime components and intensities given in Sec. IV A one can calculate the fraction of positrons annihilating in defects in the quenched specimen.
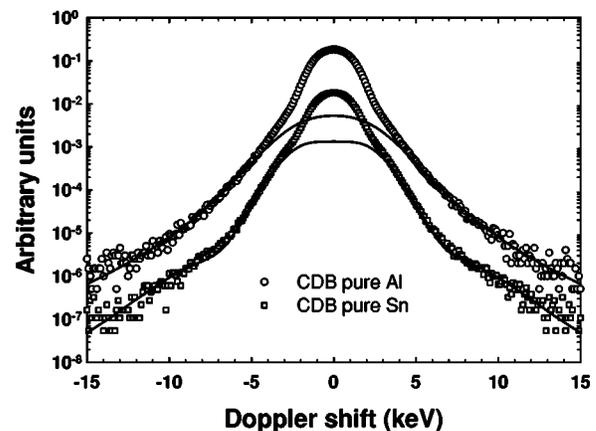
FIG. 7. Measured CDB spectra of Al and Sn combined with calculated HMP profiles (full lines). The experimental spectra of Al and Sn are normalized to the same area, but they are mutually shifted in the vertical direction.
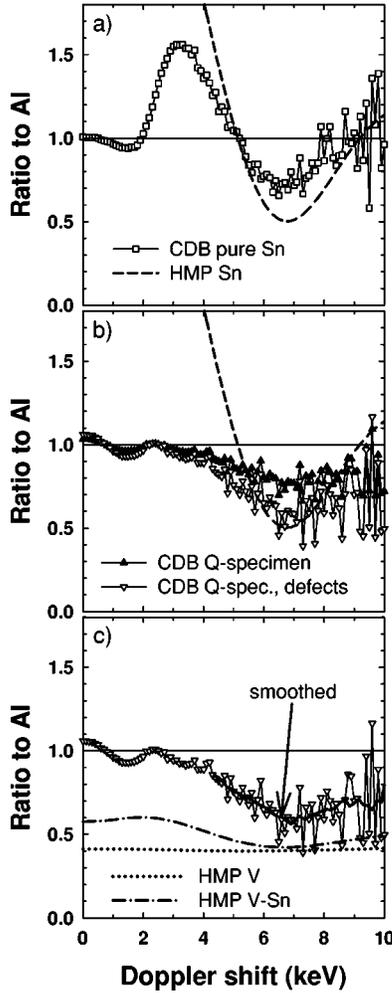
FIG. 8. The CDB/HMP ratio profiles for (a) pure Sn, (b) the quenched (Q) specimen and the corresponding defect component, and (c) V and V-Sn defects (the smoothed quenched defect profile is marked by an arrow).

First, the trapping rate can be calculated as $K=(1/\tau_B -1/\tau_2)I_2/I_1$ to be 7.52 ns^{-1}. Then, the annihilation fraction $\eta=K/(K+1/\tau_B)$ amounts to 55 %. Using this quantity one can extract the defect CDB profile from the measured spectrum of the quenched specimen. In particular, the following equation holds:

$$\varrho^Q = (1 - \eta)\varrho^{Al} + \eta\varrho^{Q,def}, \tag{10}$$

where ϱ^Q, $\varrho^{Q,def}$, and, ϱ^{Al} are, respectively, CDB profiles of the quenched specimen, its defect component, and pure Al. The resulting defect profile is also shown in Fig. 8(b). For Doppler shifts larger than ~4 keV both plotted CDB profiles exhibit similar features as that for pure Sn (a local maximum at ~3 keV and a minimum at ~7 keV). This indicates the presence of Sn atoms in the neighborhood of positron trapping sites. Furthermore, these profiles also manifest the presence of vacancylike defects because for small Doppler shifts profiles exceed the level 1. In this context it is also helpful to mention that due to the facts that in the quenched Al-Sn

specimen an apparently lower fraction of positrons annihilates with 4d electrons of Sn (due to low Sn content) and the positron overlap with Sn 4d electrons is also smaller (due to positron trapping) in comparison with the pure Sn specimen, the peak at ~3 keV of the CDB ratio profile of the quenched Al-Sn specimen is diminished compared to pure Sn.

Finally, in Fig. 8(c) the HMP profiles of V and V-Sn defects are plotted together with the defect component shown already in Fig. 8(b). The profile for the Al vacancy is rather flat without any features. In contrast, the profile for the V-Sn complex exhibits a minimum around 7 keV, similarly to pure Sn and the defect CDB profile. This fact is even more apparent when appropriate smoothing of experimental ratio curves is done [see Fig. 8(c)]. It is thus natural to identify the defect component in the quenched specimen with vacancy-Sn pairs in agreement with the above discussion based on the lifetime results. We should yet mention that the CDB defect ratio profile extracted from experiment is shifted up with respect to the calculated HMP V-Sn profile by about 0.2. We suppose that this effect as well as a similar observation for pure Sn (discussed above) are due to the fact that the theoretical approach used for electron-positron correlations does not give absolutely precise predictions of HMP profiles. However, we cannot exclude a minor influence of other impurity atoms, especially Fe, as discussed below.

Though the concentration of Fe and Si vacancy pairs was estimated to be negligible in the studied alloy (Sec. IV C), for completeness we also discuss a possible influence of Si and Fe impurities on CDB/HMP profiles. The HMP profile originating from vacancy-Si pairs should be rather flat and positioned below the profile of V-Sn as indicated by the defect free Si HMP profile shown in Fig. 2. The vacancy-Fe case requires more attention as, in principle, the corresponding CDB ratio profile could be rather similar to that for the vacancy-Sn pair. Namely, the corresponding HMP profile should also have a minimum around 7 keV. This is also indicated by our first calculations which further show that this minimum is apparently broader and is positioned higher (by about 0.1) than that for V-Sn pairs. Furthermore, the peak around 3 keV is likely to disappear and the corresponding lifetime is about 10 ps shorter than for V-Sn pairs. These features are caused by strong lattice relaxations around V-Fe pairs. On the other hand, though the experimental CDB profile does not exhibit such a broad minimum and the peak around 3 keV is apparently present, a weak contribution of vacancy-Fe pairs to the measured CDB profile plotted in Fig. 8(c) cannot be fully excluded. In conclusion, neither Si nor Fe vacancy pairs' signatures were explicitly observed experimentally and this further confirms that the effect of such pairs in the current PAS study can likely be neglected, and the CDB defect ratio profile for the quenched Al-Sn sample comes predominantly from vacancy-Sn pairs.

F. Thermal evolution of Al-Sn system

The mean diffusion length of Sn in the Al host, L_{Sn}, calculated from Eq. (3) for $t=20$ min, i.e., the time of each annealing step, is plotted in Fig. 9 as a function of temperature. The mean distance between the dissolved Sn atoms in
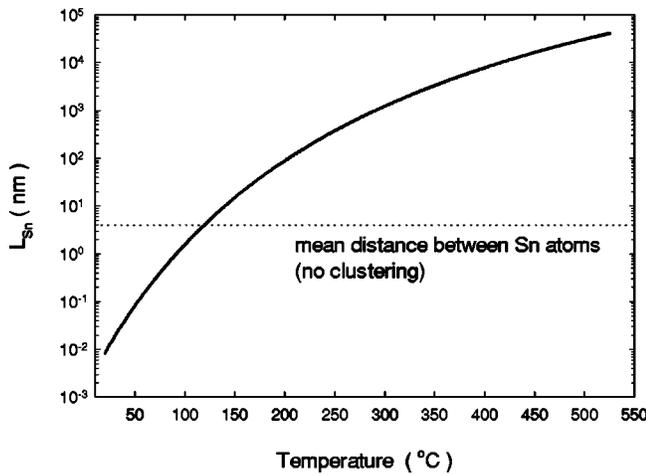
FIG. 9. The temperature dependence of the mean diffusion length L_{Sn} of Sn atoms for an annealing time of $t=20$ min. The mean distance between Sn atoms diluted in the solid solution in the quenched specimen is indicated by the dotted line. No clustering of Sn atoms during quenching was considered.

FIG. 10. The temperature (T) dependence of the equilibrium concentration of vacancies c_V^* (solid line, right vertical scale axis) and the equilibrium concentration of vacancy-Sn pairs c_{V-Sn}^* (dashed line, left vertical scale axis) in the studied Al-Sn alloy.

the quenched sample is ≈ 4 nm (dotted line in Fig. 9) under the assumption that no clustering of dissolved Sn atoms takes place during quenching. As seen in Fig. 9, the mean diffusion length of Sn becomes comparable with the distance between the dissolved Sn atoms at a temperature slightly above 100 °C. Thus the clustering of Sn atoms should start around this temperature or a little higher because some part of Sn atoms could cluster during quenching (see Sec. IV C). Simultaneously, the lifetime τ_2 starts to increase around 130 °C, see Fig. 4, and reaches 270 ps at 200 °C. The lifetime of positrons trapped at a vacancy in Sn, $\tau_V^{Sn}=274$ ps was calculated (see Table II). It is a remarkably higher value than the lifetime $\tau_V^{Al}=240$ ps of positrons trapped at a vacancy in Al. Thus one could assume that the increasing number of Sn atoms surrounding a vacancy leads to the observed increase of τ_2 because the "Al-type" vacancy surrounded initially mostly by Al atoms (only a single nearest neighbor Sn atom) transforms into a "Sn-type" vacancy surrounded predominantly by Sn atoms. Another explanation could be that positrons annihilate at free volumes at the interfaces between Sn precipitates/aggregates and the Al matrix. A CDB measurement is planned to inspect this uncertainty. The clustering of Sn atoms is reflected also by a decrease of the intensity I_2 (see Fig. 5) as the mutual distance among Sn clusters, which contain positron traps, increases.

It should be yet noted that a positron lifetime of 273 ps was calculated for positrons trapped at the Al divacancy.[33] It is also close to $\tau_2 \approx 270$ ps observed in experiment. However, it is well known[60] that divacancies as well as vacancies in Al are mobile well below room temperature. Therefore, divacancies would be quickly annealed out after quenching of the sample to room temperature. Hence, the long-term stability of the observed defects at room temperature clearly indicates that they are stabilized by Sn atoms.

According to the Al-Sn equilibrium phase diagram,[13] tin
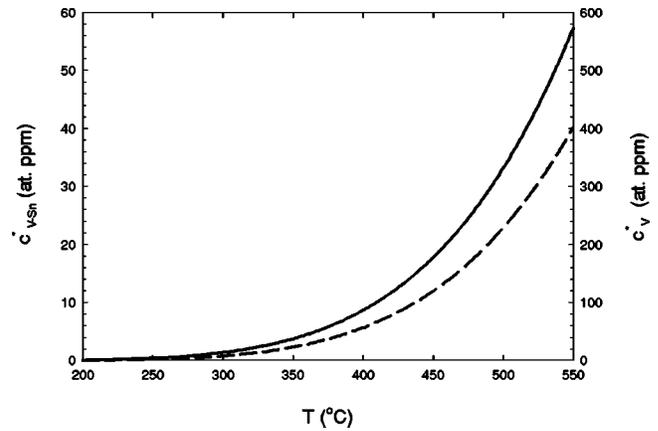
is melted and its small amount becomes dissolved in Al above 230 °C. The tin solubility in Al increases with the temperature and reaches its maximum (260 at. ppm) at ~ 600 °C (Ref. 13). The gradual dissolution of Sn precipitates with the increasing annealing temperature is likely accompanied by a release of the bound vacancies that diffuse to sinks at the samples' surface and grain boundaries. The recovery of vacancies is reflected by a decrease of the intensity I_2. However, the concentration of thermal equilibrium vacancies increases with the temperature at the same time, i.e., it represents a competing process. At temperatures above 300 °C the thermal-equilibrium concentration of vacancies becomes significant. The pairs of thermal equilibrium vacancies and the dissolved Sn atoms are formed again. The equilibrium concentration c_{V-Sn}^* of the vacancy-Sn pairs at various temperatures is given by Eq. (6), where the temperature dependence of $c_{Sn}^{dissolved}$ is considered. The temperature dependencies of c_{V-Sn}^* and c_V^* are plotted in Fig. 10. As the sample was rapidly quenched after each annealing step and subsequent PAS measurements were carried out at room temperature, the thermal vacancies not associated with Sn atoms quickly disappear after and/or during quenching and only vacancies bound to Sn atom are present in the quenched sample. The equilibrium concentration of vacancy-tin pairs c_{V-Sn}^* lies below the detection limit of PL spectroscopy (~ 1 at. ppm) at temperatures lower than 300 °C. However, it becomes important above 300 °C. The increasing number of vacancy-Sn pairs formed during annealing leads to an increase of the intensity I_2 of trapped positrons. The positron trapping rate to the vacancy-Sn pairs formed during annealing is

$$K_{V-Sn}(T) = \nu_V c_{V-Sn}^*(T). \qquad (11)$$

The intensity of trapped positrons corresponding to the trapping rate K_{V-Sn} is given by the expression

$$I_2 = \frac{K_{V\text{-}Sn}}{\tau_B^{-1} - \tau_2^{-1} + K_{V\text{-}Sn}}. \tag{12}$$

The intensity I_2 calculated from Eq. (12) is plotted in Fig. 5 by the dotted line. Clearly, it exhibits a reasonable agreement with the temperature dependence of the measured intensity I_2 at temperatures above 350 °C. This gives an apparent evidence that positrons are trapped at Sn-vacancy pairs formed during annealing. The difference between the calculated and measured intensity I_2 at the temperature interval 250–350 °C is likely due to the fact that Sn clusters were not completely dissolved yet. The lifetime τ_1 calculated from the trapping rate $K_{V\text{-}Sn}$ from the relation

$$\tau_1 = \frac{1}{\tau_B^{-1} + K_{V\text{-}Sn}} \tag{13}$$

is plotted in Fig. 4 by the dotted line. Similarly to the case of I_2 it exhibits a reasonable agreement with the measured lifetime of free positrons at temperatures above 350 °C.

G. Slowly cooled sample

Finally, we annealed a specimen at the temperature 525 °C (solution treatment) for 30 min. After annealing the specimen was not quenched, but it was slowly cooled down inside the furnace. Similarly to the quenched specimen, the PL spectrum of this slowly cooled specimen was well fitted by two exponential components. The first component, $\tau_1 = 149 \pm 3$ ps, $I_1 = 74 \pm 7$ %, comes from delocalized positrons. The second one, $\tau_2 = 211 \pm 9$ ps, $I_2 = 26 \pm 7$ %, represents the contribution of trapped positrons. Obviously, both the lifetime τ_2 and intensity I_2 lie substantially below those found in the quenched specimen (see Figs. 4 and 5). It directly indicates a significantly smaller amount of vacancies bound to Sn atoms in the slowly cooled specimen. The decrease of the vacancy concentration in the slowly cooled specimen is most probably caused by the migration of Sn-vacancy pairs to sinks (grain boundaries, dislocations) and recombination of vacancies. On the other hand, the lifetime τ_2 for the slowly cooled specimen is close to that of positrons annihilated in defect-free β-Sn (see Table II). The reason can be that due to a smaller amount of vacancies bound to Sn atoms positron annihilation inside Sn precipitates becomes important. We suppose that tin atoms may join large Sn particles (see Sec. IV B) at the beginning of the cooling process. When further cooling down the diffusivity of Sn in Al decreases as well as the concentration of vacancies. For this reason Sn atoms (either themselves or coupled to vacancies) cannot diffuse too long distance and may, thus, create small particles only (smaller than those discussed in Sec. IV B).

However, the measured CDB profile of the slowly cooled specimen (not shown here) does not exhibit any signature of Sn and any relevant impurity. After extracting the defect component from this profile (annihilation fraction 8%, see Sec. IV E), the resulting ratio profile appears to be unusable for any analysis due to a very large scatter and the above conclusions cannot be further verified.

V. CONCLUSIONS

An extensive study of the diluted Al-Sn alloy using positron-lifetime and coincidence Doppler broadening techniques was performed. The detailed information, which is useful for the understanding of the vacancy-tin interaction and its influence on the diffusion of tin atoms, was obtained. We also addressed questions concerning the clustering of Sn atoms in Al. The main results of the present work may be summarized as follows.

During the solution treatment a significant number of thermal-equilibrium vacancies is coupled to dissolved Sn atoms and vacancy-Sn pairs are formed due to a large binding energy of vacancies and tin atoms. Excess Sn atoms create large ($\sim$100 nm size) precipitates.

In the specimen quenched rapidly to room temperature the vacancy-Sn pairs are present, while the bare vacancies not associated with Sn atoms are not detected. This was found through positrons trapped at vacancies bound to Sn atoms. A clustering of Sn atoms may take place only during quenching, while no clustering of Sn atoms occurs at room temperature. Positron annihilation at V-Sn pairs prevails over annihilation at Sn precipitates.

During the subsequent annealing the clustering of Sn atoms and formation of fine Sn precipitates starts at about 130 °C. The increasing number of Sn atoms surrounding a vacancy is reflected by an increase of the lifetime τ_2 of trapped positrons. When further increasing the annealing temperature a dissolution of Sn precipitates takes place above 230 °C (melting temperature of Sn). The decreasing amount of Sn atoms surrounding a vacancy leads to a gradual decrease of the lifetime corresponding to trapped positrons. The confined vacancies become released and annealed out, which is reflected by a decrease of intensity of trapped positrons. When the annealing temperature yet increases, thermal vacancies are coupled with diluted Sn atoms and vacancy-Sn pairs are created. The contribution of the vacancy-Sn pairs created during annealing becomes important above $\sim$300 °C.

In the slowly cooled specimen the concentration of Sn-vacancy pairs is small and positron trapping at Sn particles probably dominates.

In this way the questions raised at the beginning of this article are answered. We have demonstrated that positron annihilation methods can be employed for alloys with nontrivial composition similar to those used in practical applications. In such cases combining PA experiments with computations of PA characteristics appears to be indispensable in order to interpret properly measured data. The presented study represents a first step towards investigations of Al-Cu-Sn alloys.

*Electronic address: jcizek@mbox.troja.mff.cuni.cz

†Deceased.

[1] I. Polmear, Mater. Sci. Forum **363-365**, 1 (2001).

[2] *Positron Solid State Physics*, edited by W. Brandt and A. Dupasquier (North Holland, Amsterdam, 1983).

[3] *Positron Spectroscopy of Solids*, edited by A. Dupasquier and A. P. Mills, Jr. (IOS, Amsterdam, 1995).

[4] Y. Nagai, M. Hasegawa, Z. Tang, A. Hempel, K. Yubuta, T. Shimamura, Y. Kawazoe, A. Kawai, and F. Kano, Phys. Rev. B **61**, 6574 (2000).

[5] M. A. van Huis, A. van Veen, H. Schut, C. V. Falub, S. W. H. Eijt, P. E. Mijnarends, and J. Kuriplach, Phys. Rev. B **65**, 085416 (2002).

[6] Y. Nagai, K. Takadate, Z. Tang, H. Ohkubo, H. Sunaga, H. Takizawa, and M. Hasegawa, Phys. Rev. B **67**, 224202 (2003).

[7] M. Biasini, G. Ferro, P. Folegati, and G. Riontino, Phys. Rev. B **63**, 092202 (2001).

[8] Y. Nagai, M. Murayama, Z. Tang, T. Nonaka, K. Hono, and M. Hasegawa, Acta Mater. **49**, 913 (2001).

[9] J. W. Martin, *Precipitation Hardening*, 2nd ed. (Butterworth Heinemann, Oxford, 1998).

[10] E. Matsubara and J. B. Cohen, Acta Metall. **31**, 2129 (1983).

[11] J. Faltus and K. Plaček, in *Proceedings of 6th International Metallurgic Symposium METAL 97*, edited by T. Prnka (Tanger, Ostrava, 1997), Vol. 3, p. 131.

[12] M. Cieslar, M. Hájek, J. Pelcová, I. Stulíková, and P. Vostrý, Alum. Trans. **2**, 278 (2000).

[13] A. J. McAlister, and D. J. Kahan, Bull. Alloy Phase Diagrams **4**, 167 (1983).

[14] G. Fiorito, S. Ceresara, and T. Federighi, Acta Metall. **14**, 452 (1966).

[15] H. Kimura and R. R. Hasiguti, J. Phys. Soc. Jpn. **18**, 73 (1963).

[16] M. Kato, Y. Ishida, K. Sassa, S. Uneyama, and M. Mori, J. Phys. (France) (France) **35**, C6-309 (1974).

[17] S. Uneyama, M. Taniwaki, Y. Ishida, and M. Kato, J. Phys. (France) **40**, C2-539 (1979).

[18] M. Taniwaki, S. Uneyama, and Y. Ishida, in *Point Defects and Defect Interactions in Metals*, edited by J.-I. Tamakura, M. Doyama, and M. Kiritani (University of Tokyo Press, Tokyo, 1982), p. 477.

[19] A. Vértes, Cs. Szeles, M. Z. Awad, S. Nagy, and A. Lendwai, Scr. Metall. **16**, 1229 (1982).

[20] Cs. Szeles, K. Süvegh, Z. Homonnay, and A. Vértes, Phys. Status Solidi A **103**, 397 (1987).

[21] A. Dupasquier, P. Folegati, N. de Diego, A. Somoza, J. Phys.: Condens. Matter **10**, 10 409 (1998).

[22] A. Seeger and F. Banhart, Phys. Status Solidi A **102**, 171 (1987).

[23] I. K. Mackenzie, in *Positron Solid State Physics* (Ref. 2), p. 196.

[24] K. G. Lynn, J. R. MacDonald, R. A. Boie, L. C. Feldman, J. D. Gabbe, M. F. Robbins, E. Bonderup, and J. Golovchenko, Phys. Rev. Lett. **38**, 241 (1977).

[25] M. Alatalo, H. Kauppinen, K. Saarinen, M. J. Puska, J. Mäkinen, P. Hautojärvi, and R. M. Nieminen, Phys. Rev. B **51**, 4176 (1995).

[26] F. Bečvář, L. Lešták, I. Novotný, I. Procházka, F. Šebesta, and J. Vrzal, Mater. Sci. Forum **175-178**, 947 (1995).

[27] F. Bečvář, J. Čížek, L. Lešták, I. Novotný, I. Procházka, and F. Šebesta, Nucl. Instrum. Methods Phys. Res. A **443**, 557 (2000).

[28] F. Bečvář, J. Čížek, and I. Procházka, Acta Phys. Pol. A **95**, 448 (1999).

[29] I. Procházka, I. Novotný, and F. Bečvář, Mater. Sci. Forum **255-257**, 772 (1997).

[30] R. M. Nieminen, in *Positron Spectroscopy of Solids* (Ref. 3), p. 443.

[31] M. J. Puska and R. M. Nieminen, Rev. Mod. Phys. **66**, 841 (1994).

[32] O. K. Andersen, O. Jepsen, and M. Šob, in *Electronic Band Structure and Its Applications*, edited by M. Yussouff (Springer Verlag, Heidelberg, 1987), p. 1.

[33] M. J. Puska and R. M. Nieminen, J. Phys. F: Met. Phys. **13**, 333 (1983).

[34] A. P. Seitsonen, M. J. Puska, and R. M. Nieminen, Phys. Rev. B **51**, 14 057 (1995).

[35] E. Boroński and R. M. Nieminen, Phys. Rev. B **34**, 3820 (1986).

[36] B. Barbiellini, M. J. Puska, T. Torsti, and R. M. Nieminen, Phys. Rev. B **51**, 7341 (1995).

[37] J. Kuriplach, M. Šob, G. Brauer, W. Anwand, E. -M. Nicht, P. G. Coleman, and N. Wagner, Phys. Rev. B **59**, 1948 (1999).

[38] J. Kuriplach, A. L. Morales, C. Dauwe, D. Segers, and M. Šob, Phys. Rev. B **58**, 107475 (1998).

[39] A. P. Mills, in *Positron Solid State Physics*, (Ref. 2), p. 432.

[40] J. Kuriplach, E. Dryzek, J. Dryzek, and M. šob, Acta Phys. Pol. A **95**, 605 (1999).

[41] J. Kuriplach, F. Bečvář, J. Čížek, and I. Procházka, Mater. Sci. Forum **445-446**, 132 (2004).

[42] P. Hautojärvi and C. Corbel, *in Positron Spectroscopy of Solids* (Ref. 3), p. 491.

[43] G. Kresse and J. Hafner, Phys. Rev. B **47**, 558 (1993); **49**, 147 251 (1994).

[44] G. Kresse and J. Furthmüller, Comput. Mater. Sci. **6**, 15 (1996).

[45] G. Kresse and J. Furthmüller, Phys. Rev. B **54**, 117169 (1996).

[46] T. Korhonen, M. J. Puska, and R. M. Nieminen, Phys. Rev. B **54**, 15 016 (1996).

[47] W. Brandt, in *Positron Annihilation*, edited by A. T. Stewart and L. O. Roellig (Academic Press, New York, 1967), p. 155.

[48] G. Erdélyi, K. Freitag, and H. Mehrer, Philos. Mag. **63**, 1167 (1991).

[49] W. Brandt and R. Paulin, Phys. Rev. B **5**, 2430 (1972).

[50] T. Federighi, in *Lattice Defects in Quenched Metals*, edited by R. M. J. Cotterill, M. Doyama, J. J. Jackson, and M. Meshii (Academic, New York, 1965), p. 217.

[51] K. Sassa, W. Petry, and G. Vogl, Philos. Mag. A **48**, 41 (1983).

[52] K. Maier, in *Positron Spectroscopy of Solids* (Ref. 3), p. 265.

[53] W. Shule, in *Point Defects and Defect Interactions in Metals*, edited by J.-I. Tamakura, M. Doyama, and M. Kiritani (University of Tokyo Press, Tokyo, 1982), p. 551.

[54] S. P. Ringer, K. Hono, and T. Sakurai, Metall. Mater. Trans. A **26**, 2207 (1995).

[55] S. P. Ringer and K. Hono, Mater. Charact. **44**, 101 (2000).

[56] M. Koike, K. Furukawa, J. Takamura, H. Hira, N. Yamamoto, and F. Nakamura, in *Point Defects and Defect Interactions in Metals*, edited by J.-I. Tamakura, M. Doyama, and M. Kiritani (University of Tokyo Press, Tokyo, 1982), p. 457.

[57] L. F. Modolfo, in *Aluminium Alloys: Structure and Properties* (Butterworths, London, 1976, p. 265.

[58] T. B. Massalski, *Binary Alloy Phase Diagrams* (ASM International, Metals Park, OH, 1986), Vol. 1, p. 147.

[59] S. Hirosawa, T. Sato, A. Kamio, and H. M. Flower, Acta Mater. **48**, 1797 (2000).

[60] A. Van den Beukel, in *Vacancies and Interstitials in Metals*, edited by A. Seeger, D. Schumacher, W. Schilling, and J. Diehl (North Holland, Amsterdam, 1970), p. 427.